Dynamic shape reconstruction of a notched beam by proportional observer and multi-resolution analysis

F. Saltari [1], **D. Dessi** [2], **F. Mastroddi** [1], **F. Passacantilli** [2], **E. Faiella** [2]
[1] Sapienza University of Rome, Department of Mechanical and Aerospace engineering,
Via Eudossiana 18, 00184, Rome, Italy

[2] CNR-INM Institute of Marine Engineering – National Research Council,
Via di Vallerano 139, 00128, Rome, Italy
e-mail: **daniele.dessi@cnr.it**

Abstract
A novel virtual sensing technique aimed at reconstructing the displacement field throughout the structure from pointwise measurements is here exploited for dynamic shape reconstruction of a notched beam. This estimator is a proportional observer that exploits a linear, frequency independent, relation between the estimated state-space vector and the measurements. To improve its accuracy, this concept is augmented to the definition of a sequence of proportional observers, each one acting on a signal decomposition provided by wavelet multi-resolution analysis . The considered experimental test case is a straight, uniform beam with an unmodeled stiffness and mass reduction. The strain data are provided by strain gauges positioned on the top face of the beam, whereas the estimated state variables are the time dependent coordinates of the modal expansion of the vertical displacement along the beam elastic axis. An optimization solver, which minimizes the estimation error, is employed to get the optimal gain matrix of the proposed observer.

1 Introduction

The availability of high-performance computing at different scales makes nowadays the implementation of digital twins of complex structural systems a not so far objective. For certain purposes, like structural health monitoring, the full-field description of continuous systems can be also achieved with a virtual sensing approach which brings the sensor data at the centre of the reconstruction technique. Indeed, virtual sensing aims at providing a reliable estimation of a physical variable that is not possible to measure directly. As there is no limitation in the number of virtual sensors, the present virtual sensing approach seeks to reconstruct the entire field of structural deflections and strain for continuous systems.

Typically, the problem of virtual sensing of structures has been addressed in different ways. In structural engineering, a first systematic approach to the problem of determining in real-time the applied loads, stresses and displacements motivated the development of the inverse finite element method (iFEM) [1]. The use of sub-structuring techniques (see [2]) has been also successively employed to obtain the reconstruction of the displacement field, whereas, more general approaches not necessarily limited to identify structural variables, have been typically considered in control theory applications, for instance through modal filters as in [3]. Restricting to recent years, Hwang et al. [4] proposed the use of Kalman filter to estimate the modal elastic deflections. The unknown state-space vector was made up by modal coordinates and velocities relative to a numerical model of a building; once estimated on the basis of virtual measurements, the modal coordinates allowed for providing the correspondent wind loads. Similarly, Papadimitriou et al. [5] successfully predicted the fatigue-life reduction of metallic structures by using the stress field obtained by means of Kalman filter. Lourens et al. [6] introduced the so-called augmented Kalman filter, which adds the unknown external forces to the state-space vector to be estimated. From the dynamic modelling point of view, these external forces, though unknown, were provided as the result of a random walk dynamics with an associated process noise.

Continuing the work of Gillins and De Moor [7], Lourens et al. [8] proposed a new technique to obtain a joint estimation of the state-space variables (made up by modal coordinates and velocities) as well as of the input. The joint input-response estimation exploits an algorithm similar to Kalman filter that, besides the usual tasks of measurement update and time update, considers a further step concerning the input estimation, recursively estimated by means of an unbiased minimum-variance process.

Despite of their ability to track unmeasured time-histories, all the methods that exploit Kalman filtering are not natural for second-order structural systems as highlighted by Balas [9]; the time derivative of the estimated modal coordinate (*e.g.*, relative to displacements) is not equal to the estimated velocity. This limit is magnified when unknown external forces are dominant with respect to the process and measurement noises, and consequently Balas [9] proposed a first-order observer aimed to reduce the gap. More recently, Demetriou [10] presented a natural second-order observer that utilizes a parameter-dependent Lyapunov function to ensure the asymptotic convergence of the error on the state-space variables. Among approaches based on second order observers, Hernandez [11] addressed the problem of finding the optimal observer gain by minimizing the estimation error in the frequency domain, although the observation process is naturally defined in time domain. The statistics of the noise and external loads are expressed by means of power spectral densities instead of the covariance matrices typically used in Kalman filter. This enhances the capability of observing linear (structural) systems that are intrinsically featured by their frequency domain behavior. A real-life application based on model-based observer is present in [12]).

Recently, Saltari et al. [13] have introduced the combined use of wavelet multi-resolution analysis (see Refs. [14, 15]) and proportional observer (PO) concept. The PO shares the same form with modal filters, but unlike the latter it takes into account the model structural features as well as excitation and noise statistics in building the error function; the availability of such analytical expression speeds up the error computation, and is a key point for employing error minimization procedures when dealing with large systems. This approach is then generalized to the definition of a sequence of proportional observers, each one acting on a signal decomposition provided by wavelet multi-resolution analysis, named as Multi-Resolution Proportional Observer (MR-PO).

This paper is aimed at experimentally validating the MR-PO in [13] via experimental campaign on model similar to that used for its numerical validation. The experimental testbed is a notched beam, suspended under a spring bed, with rectangular section, tested at Structural dYnamics and Diagnostics Lab (SYDLab) at CNR-INM in Rome.

The paper is organized as follows. The dynamical model of the considered mechanical system is presented in Sec. 2. Section 3 introduces the Multi-Resolution Proportional Observer as well as the correspondent analytical formulations of the estimation error. The experimental test case to which the considered method is applied is introduced in Sec. 4 whereas its analytical model is described in Sec. 5. Then, the optimization procedure to calculate the observer gain is explained in Sec.6. The numerical results accounting for the capability of the proposed method to approximate the true solution even in the points not considered for state estimation are finally discussed in Sec. 7.

2 Mechanical system modelling

In the present paper, we shall limit our attention to linear mechanical systems which can be represented in time domain, including suitable initial conditions as:

$$\mathsf{M}\ddot{\mathsf{q}} + \mathsf{D}\dot{\mathsf{q}} + \mathsf{K}\mathsf{q} = \mathsf{f} + \mathsf{w} \tag{1}$$

where $\mathsf{q} \in \mathbb{R}^N$ is a vector of generalized coordinates (nodal displacements and rotations in finite element discretization or modal amplitudes), M, D and K denote the mass, damping and stiffness $N \times N$ matrices, respectively, $\mathsf{f} \in \mathbb{R}^N$ is the external force vector and the vector $\mathsf{w} \in \mathbb{R}^N$ accounts for modelling errors in terms of process noise. The system observations are assumed to be of the form:

$$\mathsf{y} = \mathsf{S}\mathsf{q} + \mathsf{v} \tag{2}$$

where the $M \times N$ matrix S relates linearly and instantaneously the measurement vector $\mathsf{y} \in \mathbb{R}^M$ to the vector of generalized coordinates q and $\mathsf{v} \in \mathbb{R}^M$ is the measurement noise vector. More general forms of Eq. 2 have been proposed but we limit ourselves to measurements expressed in terms of displacements like strain measurements. For linear systems, it is common to consider the Fourier transform of Eqs. 1 and 2, *i.e.*,

$$-\omega^2 \mathsf{M}\tilde{\mathsf{q}} + i\omega \mathsf{D}\tilde{\mathsf{q}} + \mathsf{K}\tilde{\mathsf{q}} = \tilde{\mathsf{f}}(\omega) + \tilde{\mathsf{w}}(\omega) \tag{3}$$

$$\tilde{\mathsf{y}} = \mathsf{S}\tilde{\mathsf{q}} + \tilde{\mathsf{v}}(\omega) \tag{4}$$

where $\tilde{}$ indicates the transformed variables and the dependence on ω is highlighted only in the case of external input and noise. The frequency response function matrix $\mathsf{H}(\omega)$ for the mechanical system alone is given by:

$$\mathsf{H}(\omega) = [-\omega^2 \mathsf{M} + i\omega \mathsf{D} + \mathsf{K}]^{-1} \tag{5}$$

relating the state-space vector to the inputs, *i.e.*, $\tilde{\mathsf{q}} = \mathsf{H}(\omega)(\tilde{\mathsf{f}}(\omega) + \tilde{\mathsf{w}}(\omega))$. If the statistical features of the forcing terms in Eq. 3 as well as of the process noise are stochastic and uncorrelated to each other, the power spectral density of the state response to the stochastic inputs is obtained as follows:

$$\Phi_{\mathsf{qq}}(\omega) = \mathsf{H}^*(\omega)(\Phi_{\mathsf{ff}}(\omega) + \Phi_{\mathsf{ww}}(\omega))\mathsf{H}^{\mathsf{T}}(\omega) \tag{6}$$

where $\Phi_{\mathsf{ff}}(\omega)$ and $\Phi_{\mathsf{ww}}(\omega)$ indicate the power spectral density matrices of the inputs.

3 Multi-Resolution Proportional Observer

Let us first consider the following decomposition of the measurement vector into N_s functions spanning different time-scale ranges according to the WMRA:

$$\mathsf{y}(t) = \sum_{n=1}^{N_s} \mathsf{y}^{(n)}(t), \tag{7}$$

where the dependence on time is here highlighted for sake of clarity. For each time-scale function of the signal decomposition, one has:

$$\hat{\mathsf{q}}^{(n)}(t) = \mathsf{Q}_n \mathsf{y}^{(n)}(t). \tag{8}$$

Thus, Eqs. 7 and 8 provide the following estimation of the generalized coordinates (see Fig. 1):

$$\hat{\mathsf{q}} = \sum_{n=1}^{N_s} \hat{\mathsf{q}}^{(n)} = \sum_{n=1}^{N_s} \mathsf{Q}_n \mathsf{y}^{(n)} \tag{9}$$

Therefore, defining $\mathsf{q}^{(n)}$ as the n-th time-scale component of q obtained with the same signal decomposition (WMRA), it yields for the estimation error:

$$\mathsf{e} = \mathsf{q} - \hat{\mathsf{q}} = \sum_{n=1}^{N_s} \mathsf{q}^{(n)} - \sum_{n=1}^{N_s} \hat{\mathsf{q}}^{(n)} = \sum_{n=1}^{N_s} \left(\mathsf{q}^{(n)} - \hat{\mathsf{q}}^{(n)}\right) = \sum_{n=1}^{N_s} \mathsf{e}^{(n)} \tag{10}$$

In Eq. 10 the global error e depends on the errors at the different orders $\mathsf{e}^{(n)}$, which have the following expression:

$$\mathsf{e}^{(n)} = (\mathsf{I} - \mathsf{Q}_n \mathsf{S})\mathsf{q}^{(n)} - \mathsf{Q}_n \mathsf{v}^{(n)} \tag{11}$$

where the measurement noise is also decomposed into different contributions $\mathsf{v}^{(n)}$ corresponding to the

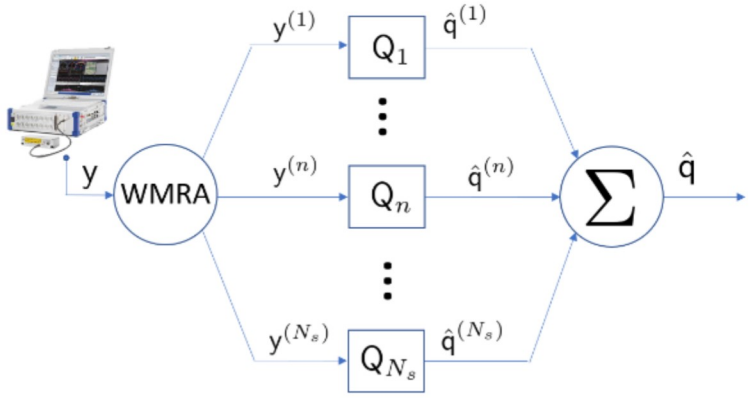

Figure 1: MR-PO plant.

selected time scales. Next, using the properties of variance (Var) and covariance (Cov), one has:

$$[\sigma^2_{\mathsf{ee}}] = \mathrm{Var}\left(\sum_{n=1}^{N_s} \mathsf{e}^{(n)}\right) = \mathrm{Cov}\left(\sum_{n=1}^{N_s} \mathsf{e}^{(n)}, \sum_{m=1}^{N_s} \mathsf{e}^{(m)}\right) = \sum_{n=1}^{N_s}\sum_{m=1}^{N_s} \mathrm{Cov}\left(\mathsf{e}^{(n)}, \mathsf{e}^{(m)}\right) \tag{12}$$

which can be further recast as:

$$[\sigma^2_{\mathsf{ee}}] = \sum_{n=1}^{N_s} \mathrm{Var}(\mathsf{e}^{(n)}) + 2\sum_{n=1}^{N_s}\sum_{m=n+1}^{N_s} \mathrm{Cov}\left(\mathsf{e}^{(n)}, \mathsf{e}^{(m)}\right). \tag{13}$$

In a more coincise form, setting $[\sigma^2_{\mathsf{e},nm}] = \mathrm{Cov}(\mathsf{e}^{(n)}, \mathsf{e}^{(m)})$, the previous equation can be expressed as:

$$[\sigma^2_{\mathsf{ee}}] = \sum_{n=1}^{N_s} [\sigma^2_{\mathsf{e},mm}] + 2\sum_{n=1}^{N_s}\sum_{m=n+1}^{N_s} [\sigma^2_{\mathsf{e},nm}] \tag{14}$$

where, recalling Eq. 11, each matrix $[\sigma^2_{\mathsf{e},mm}]$ has the following expression:

$$[\sigma^2_{\mathsf{e},nm}] = (\mathsf{I} - \mathsf{Q}_n\mathsf{S})\,[\sigma^2_{\mathsf{q},nm}]\,(\mathsf{I} - \mathsf{Q}_m\mathsf{S})^{\mathsf{T}} + \mathsf{Q}_n\,[\sigma^2_{\mathsf{v},nm}]\,\mathsf{Q}_m^{\mathsf{T}} \tag{15}$$

provided that the state-space vector q and the noise v are statistically independent, with the cross co-variance of state and noise defined as $[\sigma^2_{\mathsf{q},nm}] = \mathrm{Cov}(\mathsf{q}^{(n)}, \mathsf{q}^{(m)})$ and $[\sigma^2_{\mathsf{v},nm}] = \mathrm{Cov}(\mathsf{v}^{(n)}, \mathsf{v}^{(m)})$. Though the covariance can be computed on the time-domain signals by definition, it is more efficient to carry out its evaluation in the frequency domain due to the linearity of the observed system. Therefore, by introducing the WMRA scalar transfer function $\tilde{\gamma}^{(n)}(\omega)$ associated to the n-th scale, the Fourier transforms of the signals $\mathsf{q}^{(n)}$ and $\mathsf{v}^{(n)}$ can be obtained as:

$$\tilde{\mathsf{q}}^{(n)}(\omega) = \tilde{\gamma}^{(n)}(\omega)\tilde{\mathsf{q}}(\omega) \tag{16}$$

$$\tilde{\mathsf{v}}^{(n)}(\omega) = \tilde{\gamma}^{(n)}(\omega)\tilde{\mathsf{v}}(\omega). \tag{17}$$

Indeed, once specific wavelet and scaling functions are assigned, the WMRA based on orthogonal wavelets provides the related transfer functions $\tilde{\gamma}^{(n)}$. Therefore, the mixed-scale covariances associated to modal response and measurement noise, respectively, are given by:

$$[\sigma^2_{\mathsf{q},nm}] = \int_{-\infty}^{+\infty} \Phi_{\mathsf{qq},mn}\, d\omega = \int_{-\infty}^{+\infty} \tilde{\gamma}^{(n)}\tilde{\gamma}^{(m)}\, \Phi_{\mathsf{qq}}\, d\omega \tag{18}$$

$$[\sigma^2_{\mathsf{v},nm}] = \int_{-\infty}^{+\infty} \Phi_{\mathsf{vv},mn}\, d\omega = \int_{-\infty}^{+\infty} \tilde{\gamma}^{(n)}\tilde{\gamma}^{(m)}\, \Phi_{\mathsf{vv}}\, d\omega \tag{19}$$

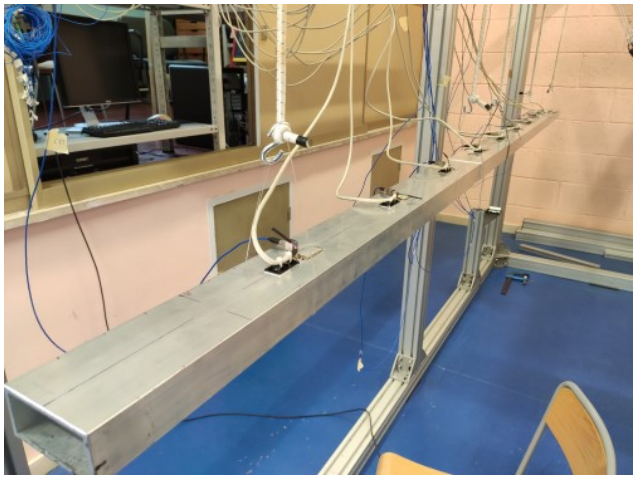

Figure 2: Tested beam at SYDLAB.

where $\Phi_{\mathsf{qq},mn}(\omega)$ and $\Phi_{\mathsf{vv},mn}(\omega)$ are the cross-spectral densities relative to the components m and n of the considered signals, which are related to the PSD matrices $\Phi_{\mathsf{qq}}(\omega)$ and $\Phi_{\mathsf{vv}}(\omega)$. Equation 14, along with Eq. 15 and the involved definitions by Eqs. 18 and 19, gives the objective function to be minimized for MR-PO. The larger number of gain matrices Q_n improves the search for the minimum. Nevertheless, it is worth noting that MR-PO maintains a quadratic form of the error covariance (see Eqs. 14 and 15).

4 Test case

As stated initially, the problem under investigation is relative to the displacement field reconstruction of a beam with a rectangular, hollow section, tested at Structural dYnamics and Diagnostics Lab (SYDLab) at CNR-INM headquarters in Rome. The beam is made of aluminum and is suspended on springs to reproduce free-free boundary conditions for the vibration modes of interest. The experimental set-up is shown in Fig. 2. The frequency of the rigid-body modes (heave and pitch) is sufficiently lower than the frequency of the two-node vertical bending mode. The beam is mostly uniform with the exception of two notches, named notch 'L' and notch 'R', respectively, placed toward the left and right end of the beam, if observed as in Fig. 2. In Fig. 3, the top view of the beam shows the position of the notches with respect to the sensor position. However, while the 'L' notch is obtained by reducing to 2mm the thickness of the entire section (half of its intact thickness), notch 'R' considers the reduction of the top side of the beam alone. The dimensions and other characteristics of the beam are reported in Table 1.

The beam is equipped with strain-gauges equally spaced with the unique exception given by an additional sensor placed close to notch 'R', with positions and numbers reported in Fig. 3. The axis orientation is inverted to be in coherent with the point of view of the beam set-up reported in Fig. 2. The strain-gauge signals are then collected by a LMS- SCADAS system at the sampling frequency of $2KHz$.

Table 1: Tested beam main dimensions and properties

Length	2.918 m	Width	0.008 m	Height	0.04 m
Thickness	0.004 m	Young modulus	68.5 GPa	Density	2728 Kg/m^3
Notch L	0.5106 m	Notch length	0.05 m	Reduced thickness	0.002 m
mid-point position				(Entire section)	
Notch R	1.985 m	Notch length	0.05 m	Reduced thickness	0.002 m
mid-point position				(Top side)	

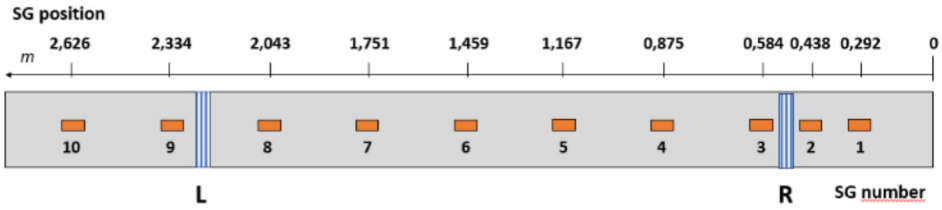

Figure 3: 2D top view of the beam with highlighted position of strain-gages and Left and Right damage.

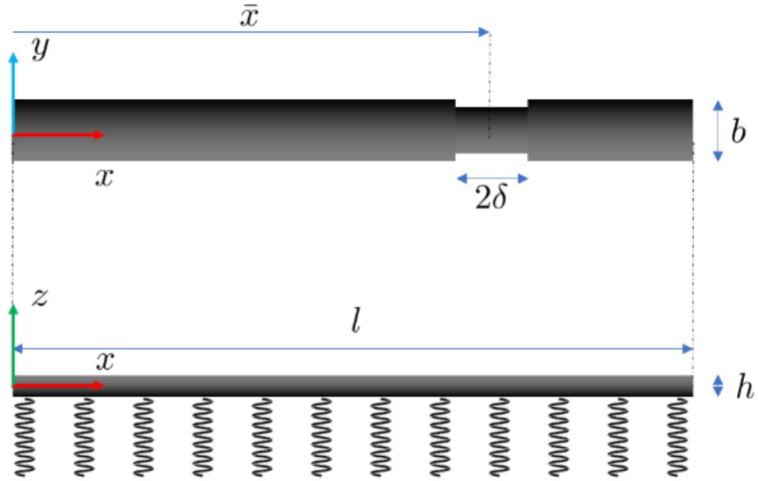

Figure 4: Reference beam model. In the example, only one notch is considered.

5 Analytic model of the experimental case study

The above theory is applied to a slender beam with a two-side notch as shown in Fig. 4. The notch represents a feature that is not included in the equations of the observed system, *i.e.*, in Eq. 1. The Euler-Bernoulli equation of a beam lying on a spring layer is:

$$\frac{\partial^2}{\partial x^2}\left[EI(x)\frac{\partial^2}{\partial x^2}\left(w+\eta_b\frac{\partial w}{\partial \bar{t}}\right)\right]+k_s\left(w+\eta_s\frac{\partial w}{\partial \bar{t}}\right)+\mu(x)\frac{\partial^2 w}{\partial x^2}=p(x) \tag{20}$$

where x, t and w are the dimensional abscissa, time and vertical displacement, respectively, $EI(x)$ and $\mu(x)$ are the piecewise constant sectional stiffness and mass, respectively, η_b is the structural damping coefficient, k_s and η_s are the spring and damping coefficients of the supporting elastic layer, respectively, and p is the external load expressed as force per unit length. The spring layer is added to represent a real structure on elastic foundations, floating condition or constrained for modal testing. The notch is represented with a reduction $\bar{b}_\delta$ of the width $\bar{b}$ of the rectangular section of the beam, while the height $\bar{h}$ is kept constant (see Fig. 4). Introducing a shape function $r_\delta(x)$, defined as $r_\delta = \bar{b}_\delta/\bar{b}$ along the notch, and equal to 1 elsewhere, width, sectional mass and stiffness ratio variations along the beam can be expressed in concise form.

The Galerkin method is exploited to transform the partial differential equation above into a system of linear ordinary differential equations by decomposing the displacement $w(x,t)$ as a sum of modal contributions, *i.e.*, $w(x,t) \approx \sum_{n=1}^{N_{modes}} q_n(t)\psi_n(x)$, where the functions $\psi_n(x)$ are the analytical normal modes of the uniform undamped free-free beam without the spring layer, including the heave and pitch rigid-body modes. From the 'true' mass M_δ, (proportional) damping D_δ and stiffness matrices $\mathsf{K}_\delta = \mathsf{K}_\delta^{(b)} + \mathsf{K}^{(s)}$, by setting $r_\delta(x) = 1$ the mass M, damping D and stiffness K matrices which define the structural model in Eq. 1 can be obtained. A more systematic description of the modelling error introduced by the notch is presented in Ref. [13].

For the sake of clarity, in the following we will refer only to the bending modes by renumbering the bending

modes or the corresponding modal coordinates from 1. The first seven modal frequencies of the considered beam (all those numerically below the Nyquist frequency of 1000 Hz) are reported in Table 2 comparing the natural frequencies evaluated experimentally with those provided by the analytical model for both notched and uniform model.

Table 2: Experimental natural frequency of the notched beam compared to the analytical solution of notched and uniform beam.

	$f_1[Hz]$	$f_2[Hz]$	$f_3[Hz]$	$f_4[Hz]$	$f_5[Hz]$	$f_6[Hz]$	$f_7[Hz]$
Experimental notched beam	33.5	89.1	175.6	288.0	419.6	578.1	757.8
Numerical notched beam	33.26	91.69	180.15	297.89	445.11	622.73	829.34
Numerical uniform beam	33.45	92.16	180.66	298.65	446.12	623.10	829.56

6 Optimal gain computation

The numerical determination of the observer gain plays a central role in the estimation techniques presented in the previous sections. It implies finding the observer gain parameters which minimize the error variance defined by Eq. 13. Thus, the present section explains how the observer gain is numerically computed according to the present observer formulation.

Suitable optimization procedures are then employed for searching the optimum gain matrix and, consequently, different optimization problems are defined in terms of objective function, design variables and constraints. The optimization problem consists in minimizing the variance matrix $\left[\sigma^2_{\mathsf{ee}}\right]$ of the estimation error on the state-space vector q. The user input consists essentially in a statistical description of disturbances and noises, *i.e.*, the covariance matrix of the measurement noise and the PSD of process noise and external excitation. For such an observer, a simple gradient-based algorithm as available in MATLAB© is employed for a full convergence to a global minimum since the objective function is quadratically dependent on the design variables. The optimizations are initialized with zero initial Q_n matrices, such that at first step $\left[\sigma^2_{\mathsf{ee}}\right] = \left[\sigma^2_{\mathsf{qq}}\right]$.

As mentioned above, the additional information required to evaluate the objective functions consist of some statistics on the measurement and process noises, as well as on the external forces, either directly provided by the covariance matrices or by the PSDs. As far as it concerns the external forces, their PSD matrix $\Phi_{\mathsf{ff}}(\omega)$ is generally derived by means of suitable spectral load models which depend on the statistical description of the environmental or operational excitation and on the transfer function from the excitation source (wind, waves, vibrations, etc) to the applied forces.

The measurement noise is modelled as white noise and featured by the sensor signal-to-noise ratio (SNR). Nonetheless, the approach foresees the presence of coloured noise to account sensors with different operating frequency range

In this experimental application, the process noise has not been modelled and, as a consequence, it has been set to zero.

7 Numerical results

As stated in the previous sections, the present application aims at estimating the full field response based on pointwise measurements provided by strain gages in presence of an unknown excitation. In Sec. 7.1, the quantities related to the measurement set-up (sensors and excitation sources) are characterized. In the same section, the implementation of multi-resolution analysis is provided along with the considered error metrics. Finally, in Sec. 7.2 the analysis of the performance in estimating the system response is dealt with for the considered methods.

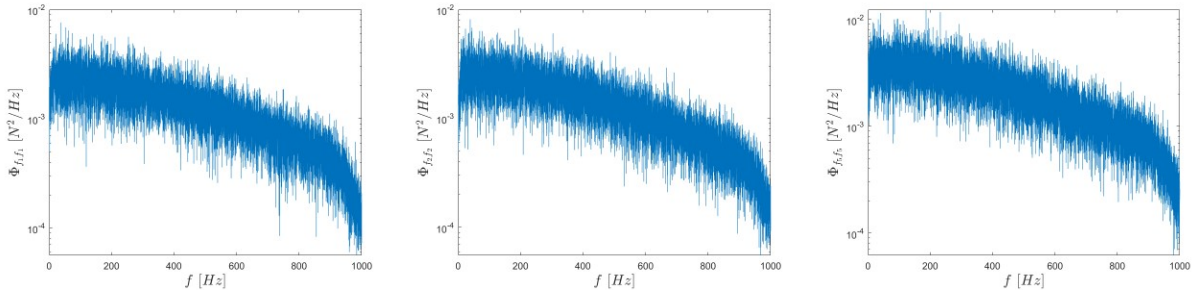

(a) $\Phi_{f_1 f_1}$. (b) $\Phi_{f_2 f_2}$. (c) $\Phi_{f_5 f_5}$.

Figure 5: Some components of synthesized power spectral density of modal external force.

7.1 Displacement field estimation

In the present application, the measurement set consists of noisy data relative to the strains on the top face of the beam at equidistant positions. The reconstruction of the elastic displacement field is done via the estimation of the modal coordinates $\hat{q}_k$ according to the following decomposition of the response:

$$\hat{w}(x,t) = \sum_{k=1}^{N_{modes}} \hat{q}_k(t)\psi_k(x), \tag{21}$$

with $\psi_k(x)$ the vertical bending modes of the uniform structure. 10 vibration modes are considered for the analysis by renumbering the bending modes from 1 to 10. The rigid-body modes are not observable since they do not generate strain response. Thus heave and pitch are excluded from the reconstruction of the deflection field.

Considering the relation between the strain and the vertical beam displacement in the linear case (small displacements), it follows:

$$y_k(t) = \frac{h}{2} \left. \frac{\partial^2 w(x,t)}{\partial x^2} \right|_{x=x_k^{(sg)}} + v_k(t), \tag{22}$$

being $h/2$ the distance between the strain sensor and the neutral axis.

The variance matrix of the measurement noise used in the error evaluation is reported below:

$$\left[\sigma_{vv}^2\right] = 0.04\mu s^2\ \mathsf{I}$$

where I is the identity matrix. The noise has been considered as equal for each sensors and uncorrelated to each other. On the other hand the process noise has been considered as unknown and for this reason set to 0.

To validate the approach in a simple experimental environment, the set goal of the present work is to provide the state response of the structure to tap test. Even though the proposed method is suitable for stochastic processes, the following criterion has been adapted to build the power spectral density associated to the external loads, that plays a key role in *training* the observer synthesis. A tap test with 155 impulsive taps in unknown positions throughout the beam has been considered to get the data for the identification of the PSD of external forces. The impact forces has been recorded by means of instrumented impact hammer. Then, the position of each impact force has been assumed to be randomly in one of the points where the strain gauges are located. These synthetic impact forces are then projected over the bending modes. Since, their number is statistically enough, it is assumed that all the considered bending modes are sufficiently excited. The PSD is then built by considering the modal forces so synthetized. Some components of this PSD are shown in Fig. 5.

The wavelet multi-resolution analysis is performed within the embedded wavelet toolbox using Daubechies

dB12 orthogonal wavelets (Ref. [14]). Specifically, $N_s = 7$ time scales are considered for the present analyses. The corresponding WMRA scalar transfer functions $\gamma_k(\omega)$ are illustrated in Fig. 6 highlighting their frequency content.

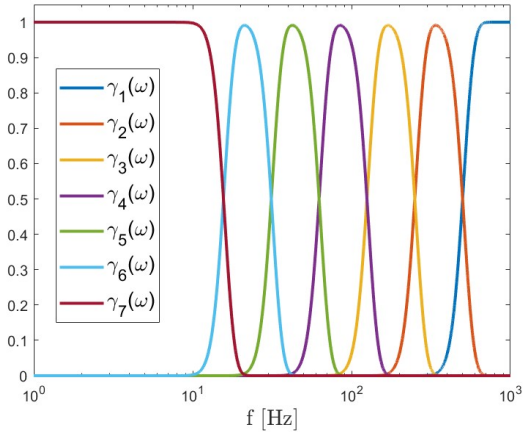

Figure 6: WMRA scalar transfer functions for the considered test case.

The fidelity level of the observation process is addressed by means of the so called *Time Response Assurance Criterium* (TRAC) (see Ref. [2]) on the strain gauge data and the covariance of the *a-posteriori* residual of measurements. In this work, the number of strain gauges used the state estimation varies to test the observer's robustness. However, the entire set of measurements, here denoted as y_c, is considered to assess the estimation performance. By taking into account the entire set of measurement vector $\mathsf{y}_c(t)$ and its *a-posteriori* estimation $\hat{\mathsf{y}}_c(t)$, the TRAC is defined as below:

$$\mathrm{TRAC}(t) = \frac{\| \, \mathsf{y}_c(t)^{\mathsf{T}} \, \hat{\mathsf{y}}_c(t) \, \|^2}{\left(\mathsf{y}_c(t)^{\mathsf{T}} \, \mathsf{y}_c(t)\right)\left(\hat{\mathsf{y}}_c(t)^{\mathsf{T}} \, \hat{\mathsf{y}}_c(t)\right)}. \tag{23}$$

The function above represents the similarity of the signal array y_c and $\hat{\mathsf{y}}_c$ with a suitable indicator in time domain and can assume values between 0 and 1 when the signals are similar. Its time-averaged value $\overline{\mathrm{TRAC}}$ is here assumed as one of the two global indicators for the quality of the estimation. Indeed, the other indicator is the trace of the covariance matrix of the *a-posteriori* measurement residual defined as $\mathrm{tr}[\mathrm{Cov}(\mathsf{y_c(t)} - \hat{\mathsf{y}}_\mathrm{c}(\mathrm{t}))]$.

7.2 Results

In order to validate the approach in Ref. [13], this work aims at estimating the modal response of the notched beam during a tap test where the position of each impact is unknown. As already defined in Sec. 7.1, not all the available measurements are used to observe the system. The most of virtual sensing/shape reconstruction techniques are particularly sensitive to the number of sensor used for estimating the state. Thus, the ultimate goal of the section is to assess the estimation capabilities of the MR-PO as well as its sensitivity to the number of strain gauges. On the other hand, the set number of modes to be tracked is ten. Besides the seven modes in Tab. 2 with a natural frequency below 1000 Hz, further 3 residual modes are taken into account. The results are provided by considering first 5 strain gauges and then 2 strain gauges. The first case takes into consideration five strain gauges uniformly spaced over the beam corresponding to the numbers 1, 4, 6, 8, 10 of Fig. 3. The modal response of the first seven modes obtained via MR-PO is shown in Fig. 7(a) in a time window between 35 s and 36 s of the considered test. On the other hand, Fig. 7(b) shows their power spectral density. The numerical simulation of a perfect, uniform, beam would present a modal response featured by the presence of only one peak of the PSD for each mode. However, the presence of unmodeled notch and of the measurement noise introduces some noise/error in the estimation procedure. Indeed, the

modal coordinate PSDs share some of the peaks of the spectrum. For instance, the first mode (blue curve) has the main peak at approximately the first modal frequency of Tab. 2. However, further peaks are visible about the second and third peaks associated to the second and third modes. A further study will investigate whether using the true modal basis reduces this effect. A comparison between the measurements of the strain gauges 3 and 5 and their *a-posteriori* estimate via MR-PO and Modal filter (MF) is then presented in Fig. 8. The considered strain gauges are out of the estimation process and result useful to check whether the state estimation provides a good agreement between real measurements and their *a-posteriori* estimates. MR-PO seems to perform well in such measurement points. The $\overline{\mathrm{TRAC}}$ (see Sec. 7.1) resulting from MR-PO estimation is 0.87. The comparison with MF is performed by projecting the vibration modes over deflection field obtained by integrating piece-wise linear function of w'' between sensors and beam edges (equivalent to natural spline approximation). In this case, MF estimate is obtained by employing all available strain gauge measurements.

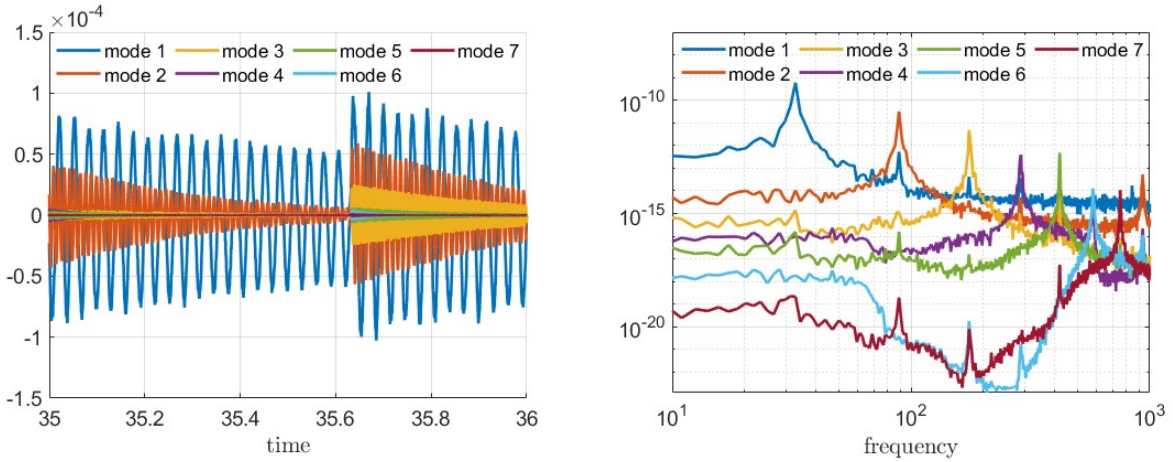

(a) Modal response

(b) PSD of modal response

Figure 7: Time histories of modal coordinates and their associated power spectral densities via MR-PO with 5 considered strain gauges.

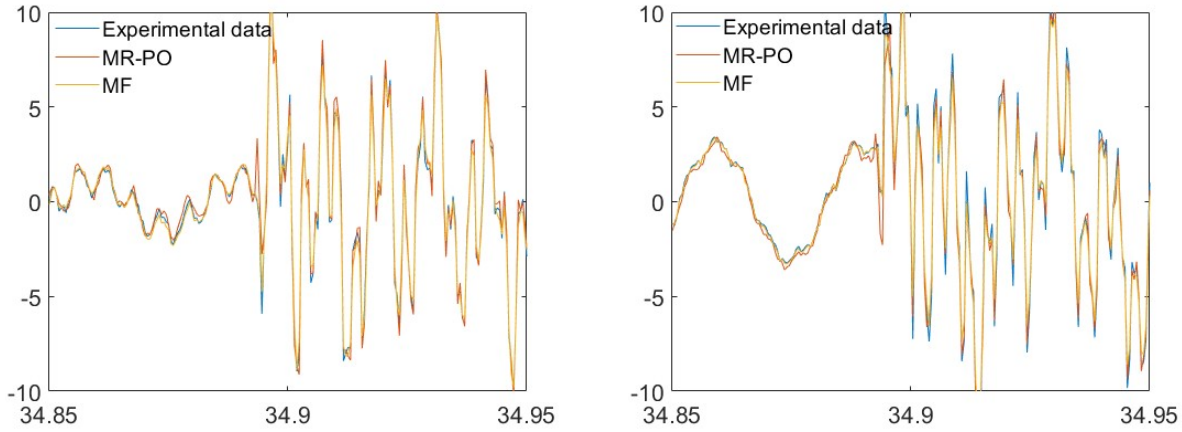

(a) Strain gauge 3

(b) Strain gauge 5

Figure 8: Comparison between the time histories of strain gauges 3 and 5 compared to their *a-posteriori* estimation via MR-PO (with 5 considered strain gauges) and MF.

The same analysis is then performed by reducing the number of strain gauges to be used for the estimation to only two, *i.e.*, strain gauges 1 and 7. The modal response obtained by this estimation is shown in Fig. 9(a)

along with their PSD in Fig. 9(b). In Fig. 9(b), it is possible to notice that the frequency content of the modal coordinates has slightly modified. The main peaks of each mode are basically the same. However, being the number of information provided by measurements much less than the previous case, the optimizer provides an observer in which Q_n components are almost zero out of the band of interest of each mode. This results in having mitigated multiple peaks. A comparison between the measurements of the strain gauges 3 and 5 and their *a-posteriori* estimate via MR-PO and Modal filter (MF) is presented in Fig. 10. This case provides a $\overline{\mathrm{TRAC}}$ value for MR-PO equal to 0.83.

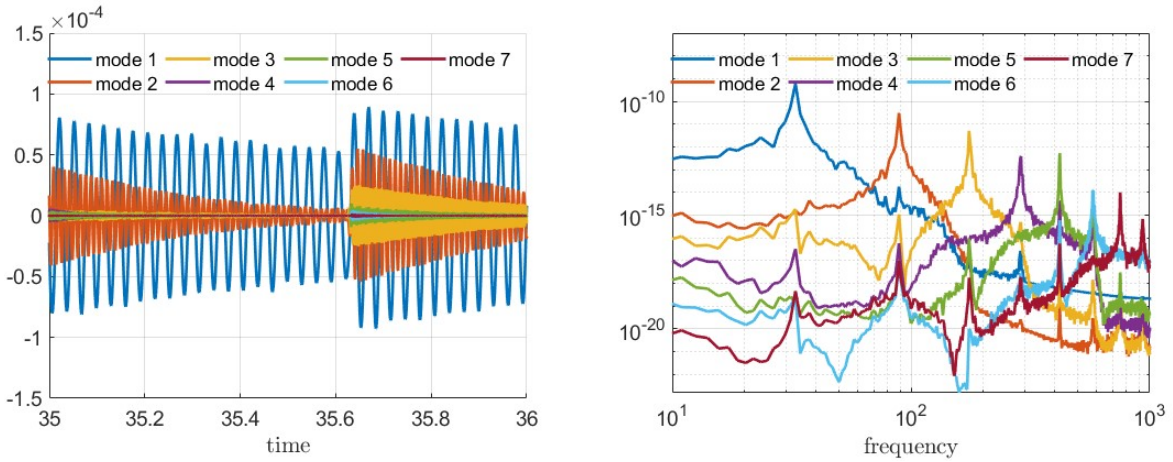

(a) Modal response

(b) PSD of modal response

Figure 9: Time histories of modal coordinates and their associated power spectral densities via MR-PO with 2 considered strain gauges.

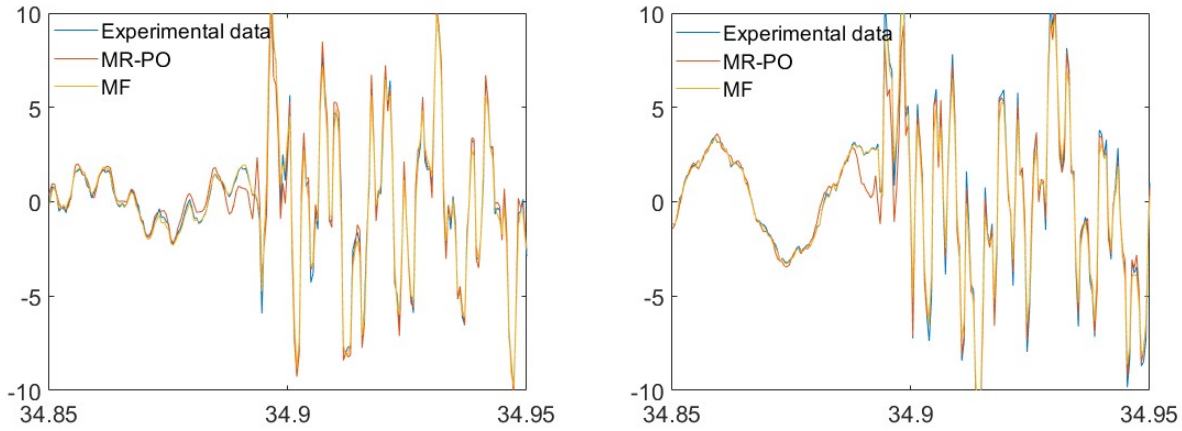

(a) Strain gauge 3

(b) Strain gauge 5

Figure 10: Comparison between the time histories of strain gauges 3 and 5 compared to their *a-posteriori* estimation via MR-PO (with 2 considered strain gauges) and MF.

Finally a convergence analysis on the number of strain gauges is carried out. The strain gauges set associated to each case of the considered sensitivity analysis is provided in Tab. 3. Thus, Fig. 11 shows the influence of the strain gauges on the state estimation performances of MR-PO as compared to MF. It is noticeable that for both MR-PO and MF the trend of covariance of the measurement residual is decreasing as the number of strain gauges involved decreases (see Fig. 11(a)). On the other hand, as expected, $\overline{\mathrm{TRAC}}$ follows the opposite trend (see Fig. 11(b)). MR-PO, as opposed to the MF, performs well independently from the number of strain gauges considered for the analysis and its performance parameters keep almost constant

with the number of strain gauges involved in the state estimation. This confirms the potential of MR-PO for shape reconstruction as already provided in Ref. [13].

Table 3: Strain gauge selection for each case.

N_{sg}	2	3	4	5	6	7	8	9
set	1 7	1 7 8	1 5 7 8	1 4 5 7 8	1 3 4 5 7 8	1 3 4 5 6 7 8	1 3 4 5 6 7 8 9	1 3 4 5 6 7 8 9 10

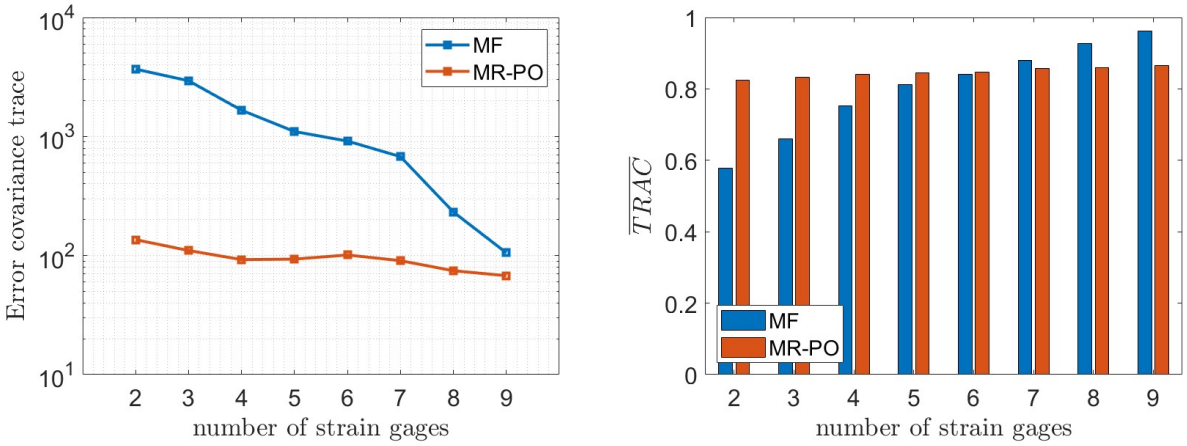

(a) Measur. residual covariance matrix sensitivity to N_{sg}.

(b) $\overline{\text{TRAC}}$ sensitivity to N_{sg}.

Figure 11: Sensitivity of the trace of the error covariance matrix and $\overline{\text{TRAC}}$ with respect to number of strain gauges

8 Conclusions

In this paper, the problem of reconstructing the vertical displacement field over an experimental beam using point-wise measurements has been addressed as a specific but meaningful example of shape reconstruction for building a digital twin based on experimental data. The so-called Multi-Resolution Proportional Observer introduced in Ref. [13], that is a generalization of the Proportional Observer introduced in the same paper as well, is employed to follow closely the different components of the tracked signals according to the signal decomposition given by wavelet multi-resolution analysis. Therefore, a detailed mathematical derivation of MR-PO has been resumed. The displacement field reconstruction is then based on a modal superposition, where the mode shapes are obtained from the numerical model of the mechanical system (mass, damping and stiffness matrices) and the time coordinates are estimated by the observer. Though recalling that the error estimation based on its analytic expression depends on the model uncertainties as well, the present procedure has some advantages: *i*) it highlights clearly the type of error dependence from the observer gain matrix, that is found to be quadratic for the MR-PO observers at the considered time-scales so facilitating the search for an absolute minimum, and *ii*) it is numerically more efficient in terms of the error computation at each iteration of the optimization process.

A beam with rectangular, hollow section with a notch tested at SYDLab at CNR-INM was then considered as testbed. Although the MR-PO in [13] is suitably developed for structure operating in stochastic environments, the goal of the work was to provide a validation of the proposed approach by estimating the modal response of the notched beam during a tap test, where the position of each impact is unknown. Measurement noise and unknown excitation have been taken into account by their statistical behavior (power spectral densities), properly specified for the considered application. The capability of accurately reconstructing the whole displacement field relies on choosing the global observer gain, in the form of a set of gain matrices,

which minimizes the variance matrix of the error between the true and the estimated state-space vector. This minimization process is carried out directly on the analytic expression of the error variance matrix which depends on the observer parameters. In the proposed real case experiment only part of the sensor data set have been considered for state estimation according to the number of strain gauges to be used for the analyses. All available sensors, including those that do not provide any information as input, were considered as control sensors on which performance metrics were computed.

Two cases, with respectively five and two strain gauges, were employed to observe the dynamic behaviour of the structure. Specifically, both cases provided reasonable results and the performance of the *worst* case (*i.e.*, the one that uses only two strain gauges) has not significantly worsened with respect to the first-one. The error sensitivity has been carried out with respect to the number of strain-gauges, thus showing that MR-PO does not experience a significant deterioration in performance due to the decrease of number of strain gauges involved in the estimation process. This has been highlighted by the comparison with the modal filter, here assumed as representative of the classical methods. This is in general true considering both the global error, evaluated with the average of TRAC function, and the covariance of the measurement residuals. The results appear rather encouraging on extending this method to the case of more complex structures for which the development of these approaches finds its ultimate motivation.

Acknowledgments

This activity was partially supported by project THALASSA (TecHnology And materials for safe Low consumption and low life cycle cost veSSels And crafts), sub-task of OR5, granted by the Italian government (ARS01_00293).

References

[1] A. Maniatty, N. Zabaras, and K. Stelson, "Finite element analysis of some inverse elasticity problems," *Journal of Engineering Mechanics*, vol. 115, no. 6, pp. 1303–1317, 1989.

[2] P. Avitabile and P. Pingle, "Prediction of full field dynamic strain from limited sets of measured data," *Shock and Vibration*, vol. 19, no. 5, pp. 765–785, 2012.

[3] L. Meirovitch and H. Baruh, "The implementation of modal filters for control of structures," *Journal of Guidance, Control, and Dynamics*, vol. 8, no. 6, pp. 707–716, 1985.

[4] J. . Hwang, A. Kareem, and W. . Kim, "Estimation of modal loads using structural response," *Journal of Sound and Vibration*, vol. 326, no. 3-5, pp. 522–539, 2009.

[5] C. Papadimitriou, C. . Fritzen, P. Kraemer, and E. Ntotsios, "Fatigue predictions in entire body of metallic structures from a limited number of vibration sensors using kalman filtering," *Structural Control and Health Monitoring*, vol. 18, no. 5, pp. 554–573, 2011.

[6] E. Lourens, E. Reynders, G. De Roeck, G. Degrande, and G. Lombaert, "An augmented kalman filter for force identification in structural dynamics," *Mechanical Systems and Signal Processing*, vol. 27, no. 1, pp. 446–460, 2012.

[7] S. Gillijns and B. De Moor, "Unbiased minimum-variance input and state estimation for linear discrete-time systems with direct feedthrough," *Automatica*, vol. 43, no. 5, pp. 934–937, 2007.

[8] E. Lourens, C. Papadimitriou, S. Gillijns, E. Reynders, G. De Roeck, and G. Lombaert, "Joint input-response estimation for structural systems based on reduced-order models and vibration data from a limited number of sensors," *Mechanical Systems and Signal Processing*, vol. 29, pp. 310–327, 2012.

[9] M. J. Balas, "Do all linear flexible structures have convergent second-order observers?," in *Proceedings of the American Control Conference*, vol. 4, pp. 2319–2323, 1998.

[10] M. A. Demetriou, "Natural second-order observers for second-order distributed parameter systems," *Systems and Control Letters*, vol. 51, no. 3-4, pp. 225–234, 2004.

[11] E. M. Hernandez, "A natural observer for optimal state estimation in second order linear structural systems," *Mechanical Systems and Signal Processing*, vol. 25, no. 8, pp. 2938–2947, 2011.

[12] F. Saltari, D. Dessi, E. Faiella, and F. Mastroddi, "Load and deflection estimation of a fast catamaran towing-tank model via reduced order modeling and optimal natural observer," in *Proceedings of ISMA 2018 - International Conference on Noise and Vibration Engineering and USD 2018 - International Conference on Uncertainty in Structural Dynamics*, pp. 3495–3509, 2018.

[13] F. Saltari, D. Dessi, and F. Mastroddi, "Mechanical systems virtual sensing by proportional observer and multi-resolution analysis," *Mechanical Systems and Signal Processing*, vol. 146, 2021.

[14] I. Daubechies, *Ten lectures on wavelets*. Society for Industrial and Applied Mathematics, 1992.

[15] S. G. Mallat and G. Zhang, "Matching pursuits with time-frequency dictionaries," *IEEE Transactions on Signal Processing*, vol. 41, pp. 3397–3415, 1993.